Polymer Chemistry

ROYAL SOCIETY OF CHEMISTRY

PAPER

View Article Online
View Journal | View Issue

Cite this: *Polym. Chem.*, 2023, **14**, 2088

Novel multi-material photo-curable resins containing high-performance photoinitiating systems and nano additives dedicated to 3D-VAT printing†

Magdalena Jankowska,[a] Anna Chachaj-Brekiesz,[b] Klaudia Trembecka-Wójciga,[c] Anna Jarzębska,[c] Monika Topa-Skwarczyńska,[a] Maciej Pilch[a] and Joanna Ortyl *[a,d,e]

Herein the suitability of new 9-[(*E*)-2-phenyl]anthracene and 9-[(*E*)-2-phenyl]phenanthrene derivatives for the role of photosensitizers of diphenylidonium salts to initiate various types of photopolymerization processes using UV- and Vis-LED light sources were presented. The usefulness of the investigated compounds for initiating the cationic photopolymerization of epoxy monomer, radical photopolymerization of an acrylate monomer, and hybrid photopolymerization were tested. The versatility of two-component initiating systems has been verified. The possibility of initiating the process of photopolymerization of resins with the addition of nanoparticles (such as titanium oxide or zinc oxide) was also checked, from which at a subsequent stage of research an attempt was made to obtain photo-curable nanocomposites. To date, literature reports on the preparation of photo-curable nanocomposites refer to two-component initiator systems that are used to initiate hybrid photopolymerization, where the process occurs according to a radical mechanism. The following work presents initiating systems that were also used to initiate the photopolymerization of hybrid resins with the addition of nanoparticles, for which photopolymerizing monomers were used simultaneously according to the radical and cationic mechanism. The use of anthracene and phenanthrene derivatives in combination with the iodonium salt allows for increased process initiation efficiency. Following current trends, it was decided to test the suitability of newly developed two-component initiator systems based on 9-[(*E*)-2-phenylethenyl]anthracene and 9-[(*E*)-2-phenylethenyl]phenanthrene derivatives for 3D printing applications in digital light processing technology for which low-budget devices were used. The main aspect discussed in the following work is the formation of photo-curable polymer nanocomposites.

Received 20th December 2022,
Accepted 8th March 2023

DOI: 10.1039/d2py01583h

rsc.li/polymers

Introduction

Photochemistry and consequently radiation-initiated polymerization processes play an extremely important role in materials engineering.[1–4] Photopolymerization processes are widely used in many industries including biomedical engineering,[5–11] automotive[12,13] and dentistry.[10,14,15] These processes are currently rapidly expanding with technologies related to forming 3D models using light-initiated 3D printing.[16–23] Photopolymerization is also frequently used in the polygraphic industry to obtain photo-cure UV varnishes and inks.[24,25] The wide range of applications of this process is mainly due to its speed and the fact that the process is not harmful to the environment.[26–30]

Especially crucial in photopolymerization processes are initiators, which are responsible for the efficiency of the process and the final product properties. Generally, these photopolymerization initiators can be divided according to their effect mechanism into photoinitiators of the first and second types.[31–34] Photoinitiators of the first type undergo photo fragmentation under the influence of radiation. This group may include benzoin derivatives,[35,36] acylphosphine oxides,[37–39] benzylketals[40] and α-hydroxyalkylphenones.[41,42]

[a]*Department of Biotechnology and Physical Chemistry, Faculty of Chemical Engineering and Technology, Cracow University of Technology, Warszawska 24, 31-155 Cracow, Poland. E-mail: jortyl@pk.edu.pl*
[b]*Faculty of Chemistry, Jagiellonian University, Gronostajowa 2, 30-387 Cracow, Poland*
[c]*Institute of Metallurgy and Materials Science, Polish Academy of Sciences, Reymonta 25, 30-059 Cracow, Poland*
[d]*Photo4Chem Lea 114, 30-133 Cracow, Poland*
[e]*Photo HiTech Ltd, Bobrzynskiego 14, 30-348 Cracow, Poland*
† Electronic supplementary information (ESI) available. See DOI: https://doi.org/10.1039/d2py01583h

The second type of photoinitiators requires the presence of a co-initiator to create reactive species (radicals) to initiate the photopolymerization process. For the role of co-initiators, tertiary amines are usually employed. Ketone derivatives are used as photoinitiators of the second type, among which benzophenone,[43,44] thioxanthone[45–48] or camphoroquinone[49,50] are distinguished.

Efforts are still being made to research new initiator systems for photopolymerization processes, mainly focused on two-component initiator systems. A variety of functional initiators have been developed for photochemical applications. Recently, more and more attention has been focused on terphenyl derivatives, which find applications in photochemistry as photosensitizers in two component initiating systems and also as fluorescent sensors. A 2015 literature report on compounds with the *m*-terphenyl skeleton (1-amino-2,6-dicyano-3,5-diphenylbenzene derivatives).[51] These compounds were used as fluorescent molecular probes to monitor the cationic photopolymerization process using the FPT method (Fluorescence Probe Technology). Based on the study, the dual nature of *m*-terphenyls was established, and the suitability of these compounds for the role of fluorescence sensors as well as photosensitizers of diphenyliodonium salt was demonstrated. In 2016, Assi Al Mousawi and co-workers proposed a new series of photoinitiators based on the *m*-terphenyl backbone.[52] In this work, new photoinitiators (*meta*-terphenyl scaffold) are suggested for cationic free radical-promoted epoxy polymerization under visible light using light-emitting diodes at 405, 455 and 470 nm. Based on the experiments, the photoinitiation ability of the proposed systems was demonstrated. In 2020, the sensitizing properties of 2-(diethylamino)-4,6-diphenyl-benzene-1,3-dicarbonitrile during the initiation of cationic, radical and hybrid photopolymerization, and the suitability of the proposed two component systems (*m*-terphenyl derivatives/diphenyliodonium salt) for 3D printing was demonstrated.[53]

Interesting photochemical properties can also be observed for naphthalene and its derivatives. Xiao in his work presented the group of compounds based on naphthalene backbone with radiation absorption up to the visible range.[54] In this work, he proved that naphthalene derivatives combined with iodonium salt or *N*-vinylcarbazole are capable of initiating different types of photopolymerization processes, *i.e.* cationic, radical, hybrid or thiol–ene photopolymerization using a low-intensity light source. Another work of French researchers concerns the application of naphthalene derivatives in three-component initiating systems.[55] The study demonstrated the high performance of naphthalene derivatives in three component photoinitiating systems for initiating radical photopolymerization, and also showed the suitability of the studied systems for 3D printing.

Moreover, anthracene derivatives, due to their highly attractive photophysical, photochemical and biological properties, have a huge application spectrum. These compounds are widely used in organic materials and in organic light-emitting diode OLEDs as well as in polymer materials. In 2021, Liu presented two-component initiating systems based on a chalcone-anthracene scaffold and iodonium salt for initiating cationic photopolymerization.[56] The anthracene derivatives exhibited good absorption properties, which led to high initiation efficiency of the photopolymerization process using light sources in the visible range. An interesting application of anthracene derivatives is their use to the role of emitters in the triplet–triplet annihilation upconversion. The development of this process is extremely important as it may find applications in drug delivery as well as bioimaging. In 2019, photon upconversion from near-infrared to blue light was described, where a commercially available compound 9,10-bis[((triisopropyl)silyl) ethynyl]anthracene was used as an annihilator.[57] The anthracene derivative used proved to be a highly efficient annihilator in the triplet–triplet annihilation upconversion. Interestingly, anthracene derivatives are also used in biology, where their properties such as antibacterial and anti-inflammatory are mainly used. In the 2019 paper, new anthracene derivatives that exhibit antimicrobial activity were presented.[58] Similar to anthracene compounds, phenanthrene derivatives are also known in the literature. In 2021, two reactive phenanthrene derivatives: 4-(1*H*-phenanthrol [9,10-*d*]imidazole-2-yl) benzaldehyde and 6,9-dimethoxyphenanthro[9,10-*c*]furan-1,3-dione, which have found application as fluorescent markers in fluorescence microscopy.[59]

In this work, the suitability of new anthracene and phenanthrene derivatives for the role of photosensitizers in two-component initiating systems was investigated. Moreover the suitability of prepared photo-curable resins for 3D printing in DLP technology were presented. The applicability of the new initiating systems for initiating hybrid photopolymerization in the presence of various nano-additives was tested, and a further study attempted to obtain composites from photocurable formulations. The versatility of the performance of the investigated new initiator systems was verified, and the possibility of preparing polymer nanocomposites from resin formulations that polymerize according to the radical mechanism, as well as the radical-cationic one, was also tested.

Experimental

The nine 9-[(*E*)-2-phenylethenyl]anthracene derivatives and the nine 9-[(*E*)-2-phenylethenyl]phenanthrene derivatives, differentiated by the type and nature of the substituent located in the second phenyl ring, for their role as photosensitizers of diphenyliodonium salt (SpeedCure 938) for efficient initiation of different types of photopolymerization process were tested. This group included the following compounds: 9-[(*E*)-2-phenylethenyl]anthracene (ANT-H), 9-[(*E*)-2-(4-cyanophenyl)ethenyl] anthracene (ANT-CN), 9-[(*E*)-2-[4-(methylsulfanyl)phenyl]-ethenyl]anthracene (ANT-SCH_3), 9-[(*E*)-2-([1,1′-biphenyl]-4-yl) ethenyl]anthracene (ANT-C_6H_5), 9-[(*E*)-2-(4-methylphenyl) ethenyl]anthracene (ANT-CH_3), 9-[(*E*)-2-(4-methoxyphenyl) ethenyl]anthracene (ANT-OCH_3), 9-[(*E*)-2-(2-pyridyl)ethenyl] anthracene (ANT-PYR), 9-[(*E*)-2-(4-chlorophenyl)ethenyl]anthracene (ANT-Cl), 9-[(*E*)-2-(4-fluorophenyl)ethenyl]anthracene

(ANT-F), 9-[(*E*)-2-phenylethenyl]phenanthrene (FEN-H), 9-[(*E*)-2-(4-cyanophenyl)ethenyl]phenanthrene (FEN-CN), 9-[(*E*)-2-[4-(methylsulfanyl)phenyl]ethenyl]phenanthrene (FEN-SCH_3), 9-[(*E*)-2-([1,1′-biphenyl]-4-yl)ethenyl]phenanthrene (FEN-C_6H_5), 9-[(*E*)-2-(4-methylphenyl)ethenyl]phenanthrene (FEN-CH_3), 9-[(*E*)-2-(4-methoxyphenyl)ethenyl]phenanthrene (FEN-OCH_3), 9-[(*E*)-2-(2-pyridyl) ethenyl]phenanthrene (FEN-PYR), 9-[(*E*)-2-(4-chlorophenyl) ethenyl]phenanthrene (FEN-Cl), 9-[(*E*)-2-(4-fluorophenyl)ethenyl] phenanthrene (FEN-F) (Fig. 1 and 2). Stuctures of the compounds were confirmed by analyzing ^{1}H NMR (Fig. S.1–S.18†).

As commercial materials in two-component initiating systems were used: bis-(4-*t*-butylphenyl)iodonium hexafluorophosphate (SpeedCure 938, Lambson Ltd) and methyl diethanolamine (MDEA, Sigma Aldrich). In additional, diphenyliodonium salt SpeedCure 938 was used as a reference initiator. The following monomers were used to study the kinetics of the photopolymerization process and for 3D printing: 3,4-epoxycyclohexylmethyl-3,4-epoxycyclohexane-carboxylate (CADE, Lambson Ltd), trimethylolpropane triacrylate (TMPTA, Sigma Aldrich), 3,4-epoxycyclohexylmethyl methacrylate (M100, Sigma Aldrich), bisphenol A ethoxylate diacrylate (BEDA, Sigma Aldrich) and 2-hydroxyethyl methacrylate (HEMA, Sigma Aldrich). Structures of the used compounds were shown in ESI (Fig. S.19†). In this study nano additives such as zinc oxide (ZnO, Sigma Aldrich, 20 nm nanoparticles size), aluminium doped zinc oxide (AlZnO, 20–40 nm nanoparticles size, US

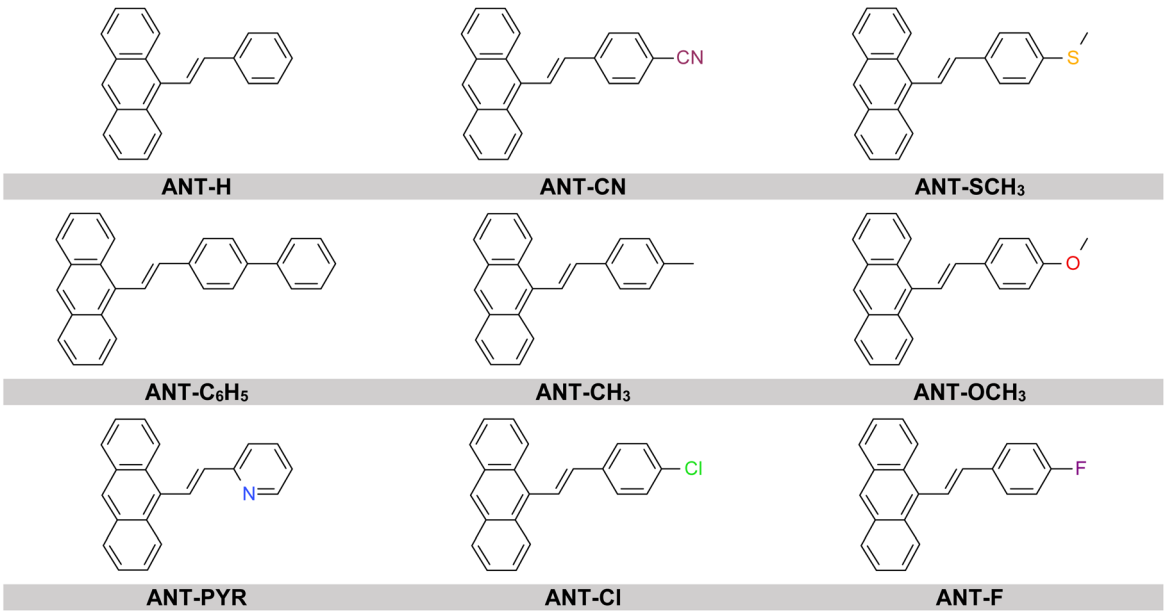

Fig. 1 Structures of 9-[(*E*)-2-phenylethenyl]anthracene derivatives.

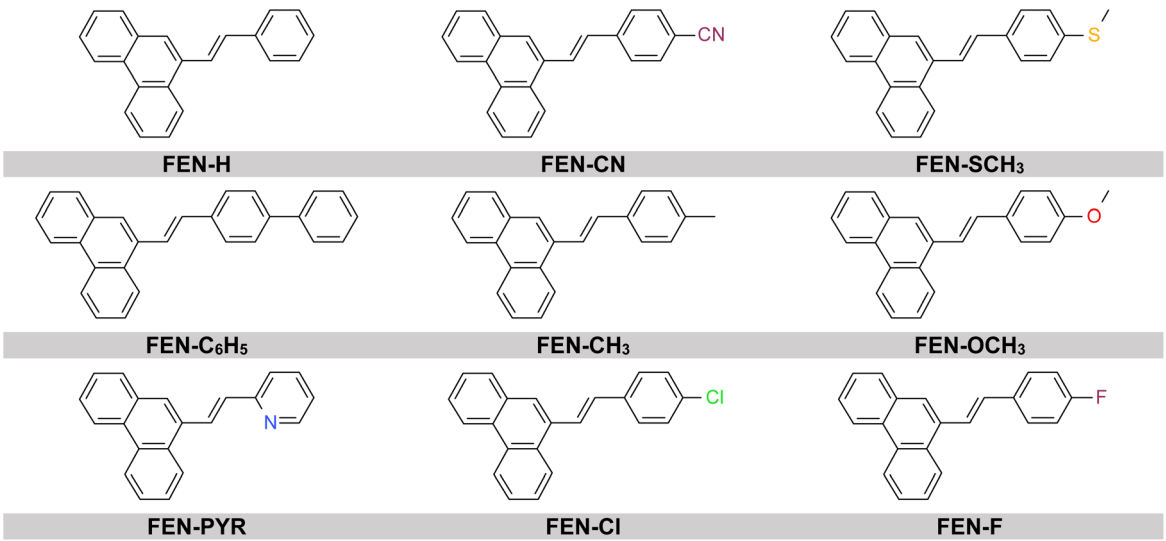

Fig. 2 Structures of the 9-[(*E*)-2-phenylethenyl]phenanthrene derivatives.

Research Nanomaterials, Inc.), titanium(IV) oxide (TiO_2, anatase, Sigma Aldrich), halloysite nanoclay ($Al_2Si_2O_5(OH)_4 \cdot 2H_2O$, Sigma Aldrich) were also used.

Spectroscopic properties

Measurements of absorbance spectra. For absorbance studies, the miniature SilverNova® TEC spectrometer equipped with a CCD array (manufactured by StellarNet Inc., USA) with a spectral range of 190 nm to 1100 nm was used. Solutions of 9-[(*E*)-2-phenylethenyl]anthracene and 9-[(*E*)-2-phenylethenyl]phenanthrene derivatives in acetonitrile were placed in a quartz cuvette (optical path length 1 cm). The light source for absorbance measurements was an SL5 deuterium–halogen lamp manufactured by StellarNet Inc.

Measurements of emission and excitation spectra and fluorescence quenching. Emission and excitation spectra as well as fluorescence extinction measurements were performed using the Quanta Master™ 40 spectrofluorimeter (Photon Technology International, Canada) equipped with a xenon lamp manufactured by the Photon Institute of Krakow. Test solutions were placed in a quartz cuvette with an optical path length of 1 cm. For fluorescence quenching tests, iodonium salt was used as a quencher, which was added in portions of 1.5–60 mg.

Fluorescence lifetime measurement

Fluorescence lifetimes were recorded using the EasyLife™ X spectrophotometer (from Photon Technology International (PTI), now part of Horiba) when excited with a light length of 310 nm. Ludox® colloidal silica solution (Sigma Aldrich) strongly diluted in water was used as a reference. Fluorescence lifetimes were estimated by fitting decay curves using a deconvolution procedure in fluorescence fading analysis software. The fluorescence decay curves were fitted using an exponential function to obtain the fluorescence lifetime τ.

Monitoring the kinetics of photopolymerization processes by real-time FT-IR

The apparatus for monitoring the kinetics of photopolymerization processes consisted of a NICOLET™ iS™ 10 spectrometer manufactured by Thermo Fisher Scientific, which was equipped with a horizontal attachment. Various UV-LEDs and Vis-LEDs were used as light sources, which emitted radiation perpendicular to the surface of the test sample with a length of:

- λ_{max} = 365 nm (M365L2 Thorlabs; light intensity on the sample surface: 18.6 mW cm^{-2})
- λ_{max} = 405 nm (M405L3 Thorlabs; light intensity on the sample surface: 26.5 mW cm^{-2})
- λ_{max} = 420 nm (M420L3 Thorlabs; light intensity on the sample surface: 5.5 mW cm^{-2})

Spectra were recorded in OMNIC software. Measurements were performed in a light-limited room at a room temperature of 25 °C. The distance from the end of the optical fibre to the surface of the sample was 2.1 cm.

The following eqn (1) was used to determine the degree of conversion of the monomers:[60,61]

$$\text{Conversion} = \left(1 - \frac{A_{\text{after polymerization}}}{A_{\text{before polymerization}}}\right) \times 100[\%] \quad (1)$$

where: $A_{\text{before polymerization}}$ is an area of the absorbance peak characteristic for used monomer and type of photopolymerization before polymerization process; $A_{\text{after polymerization}}$ is an area of the same absorbance peak, but after polymerization process.

Cationic photopolymerization of CADE monomer

Photocurable compositions to the cationic photopolymerization process included: 0.1% by weight 9-[(*E*)-2-phenylethenyl]anthracene/9-[(*E*)-2-phenylethenyl]phenanthrene derivatives, 1% by weight SpeedCure 938 and 3,4-epoxycyclohexylmethyl-3,4-epoxycyclohexane-carboxylate (CADE monomer). Measurements were carried out under aerobic conditions on a pastille made of barium fluoride (thickness 25 μm). Kinetics of the cationic photopolymerization process was monitored on the basis of a decrease in the band area located between wavenumbers 770 cm^{-1} and 820 cm^{-1}, the maximum occurs at the value equal to 790 cm^{-1} (the band corresponding to the occurrence of epoxy groups).

Radical photopolymerization of TMPTA monomer

To measure the kinetics of the radical photopolymerization process, compositions consisting of the following components were prepared: 9-[(*E*)-2-phenylethenyl]anthracene/9-[(*E*)-2-phenylethenyl]phenanthrene derivative (0.1% by weight), SpeedCure 938 (1% by weight), trimethylolpropane triacrylate (TMPTA monomer). Measurements were carried out under anaerobic conditions (between two polypropylene films, thickness 25 μm). Kinetics of the radical photopolymerization process was monitored on the basis of the disappearance of the band corresponding to the occurrence of double bonds (1635 cm^{-1}).

Hybrid photopolymerization of CADE/TMPTA/M100 monomers

For investigation of the process of hybrid photopolymerization, compositions with monomers polymerizing according to the cationic and radical mechanism were prepared. The photocurable hybrid compositions included the following monomers: 3,4-epoxycyclohexylmethyl-3,4-epoxycyclohexane-carboxylate/trimethylolpropane triacrylate/3,4-epoxycyclohexylmethyl methacrylate (2/2/1 by weight). The two-component initiating system contained: 9-[(*E*)-2-phenylethenyl]anthracene/9-[(*E*)-2-phenylethenyl]phenanthrene derivative (0.1% by weight) and SpeedCure 938 (1% by weight). The study was conducted in 3 various methods. Initially, studies were conducted under aerobic conditions on a pastille (BaF_2 pastille, thickness 25 μm, thin films). The disappearance of the band characteristic of epoxy groups (790 cm^{-1}) and double bonds (1635 cm^{-1}) was observed. Next, measurements were carried out under lami-

nated conditions (between PP films, thickness 25 μm, thin films). The last method of the study was to conduct measurements under anaerobic conditions on rings (Ø = 9.80 mm, thickness 1.16 mm, thick layers). Monomer conversion degrees were determined on the basis of the band decay located at the wavenumber 3700 cm^{-1} (epoxy groups) and 6165 cm^{-1} (double bonds). The method of applying samples in each method is shown in Scheme 1.

Hybrid photopolymerization of HEMA/BEDA monomers

The hybrid compositions, wherein both monomers polymerize according to the radical mechanism, comprise the following monomers: bisphenol A ethoxylate diacrylate (BEDA) and 2-hydroxyethyl methacrylate (HEMA) (7/3). The two-component initiator system included: the corresponding 9-[(*E*)-2-phenylethenyl]anthracene/9-[(*E*)-2-phenylethenyl]phenanthrene derivative (0.1% by weight), SpeedCure 938 (1% by weight). The kinetics of the hybrid photopolymerization process was monitored by the change in the area of the localized band between the wavenumber 6130 cm^{-1} and 6200 cm^{-1} (band maximum 6165 cm^{-1}). Measurements were conducted under anaerobic conditions in the ring (Ø = 9.80 mm, thickness 1.16 mm, thick layers). On the basement of the original composition (HEMA/BEDA: 3/7 and photosensitizer/IOD (0.1/1% by weight)), further compositions containing nanoadditives were prepared: (a) 3% w/w halloysite nanoclay, (b) 3% w/w halloysite nanoclay and 3% w/w MDEA, (c) 1% w/w AlZnO, (d) 1% AlZnO w/w and 3% w/w MDEA, (e) 1% w/w ZnO, (f) 1% w/w ZnO + 3% w/w MDEA, (g) 0.1% w/w TiO_2, (h) 0.1% w/w TiO_2 + 3% w/w MDEA.

Jacob working curves

Jacob's working curves were used to determine printing parameters such as critical energy (E_c – energy required to initiate photopolymerization process) and curing light penetration depth (D_p). The following formula (2) was used to determine the above parameters:[62,63]

$$C_d = D_p \ln\left[\frac{E_0}{E_c}\right] \quad (2)$$

C_d is the thickness of one layer of cured resin; E_0 is the energy required to cure the resin.

The critical energy (the point of intersection of the graph with the *X*-axis) and the light penetration depth (the slope of the obtained curve) were determined based on the $C_d = f(E_0)$ diagram.

Laser 3D printouts (direct ink writing)

A laser engraver (NEJE DK-8-KZ) was used to obtain 3D prints using laser technology. Prints were obtained at a light intensity of 1500 mW cm^{-2} and a wavelength of λ = 405 nm (spot size of 0.075 mm). Various light-curing compositions were tested: 9-[(*E*)-2-phenylethenyl]anthracene (0.1% by weight) + SpeedCure 938 (1% by weight) and mixture of monomers: CADE/TMPTA/M100 (2 w/w/2 w/w/1 w/w).

DLP 3D printouts

Anycubic Photon Mono X printer (Anycubic, China) with an averaged light output of 15.63 mW cm^{-2} was used to obtain prints by DLP (digital light processing). Three-dimensional objects were designed using Fusion360® software (by AutoDesk). The following compositions were examined: ANT-CH_3/IOD (0.1/1% by weight) and HEMA/BEDA (3/7); ANT-CH_3/IOD (0.1/1% by weight) and mixture of monomers HEMA/BEDA (3/7) and nanoparticle TiO_2 (0.1% by weight); ANT-SCH_3/IOD (0.1/1% by weight) and mixture of monomers CADE/TMPTA/M100 (2/2/1), ANT-SCH_3/IOD (0.1/1 w/w) and mixture of monomers CADE/TMPTA/M100 (2/2/1) and nanoparticle 0.1% TiO_2.

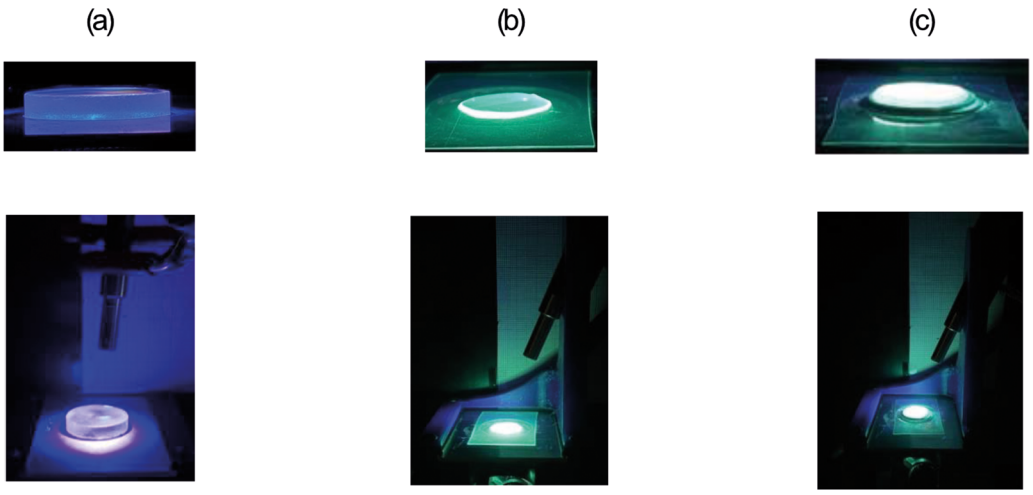

Scheme 1 Images of the sample during measurements of photopolymerization kinetics under various conditions: (a) air conditions on a pastille (BaF_2 pastille, thickness 25 μm, thin films); (b) laminated conditions (between PP films, thickness 25 μm, thin films); (c) anaerobic conditions on rings (Ø = 9.80 mm, thickness 1.16 mm, thick layers).

Optical microscopy

OLYMPUS DSX1000 optical microscope was used to observe the generated 3D objects and take 2D and 3D photographs.

Scanning electron microscopy

The morphology characterization of 3D printed structures was performed by scanning electron microscopy (SEM). The samples were sputter coated with a carbon thin film and imaging was performed using FEI E-SEM XL30 with an acceleration voltage of 10 kV and electron beam current of 4.0 nA.

Results and discussion

Spectroscopic properties

To investigate the spectroscopic properties of 9-[(*E*)-2-phenylethenyl]anthracene and 9-[(*E*)-2-phenylethenyl]phenanthrene derivatives absorbance, fluorescence quenching, fluorescence lifetime, emission and extinction measurements in acetonitrile were performed. The following graphs show the absorption characteristics of the studied compounds (Fig. 3).

The experiments showed that the absorbance of 9-[(*E*)-2-phenylethenyl]anthracene derivatives reaches up to about 450 nm. However, 9-[(*E*)-2-phenylethenyl]phenanthrene derivatives show a hypochromic shift compared with the analogous anthracene derivatives and absorb radiation in the visible range reaching up to about 420 nm.

Among the 9-[(*E*)-2-phenylethenyl]anthracene derivatives, the best spectroscopic properties (*i.e.*, absorption range extending into the visible range up to a wavelength of 460 nm and a molar extinction coefficient of 17 527 $dm^3\ mol^{-1}\ cm^{-1}$ at 389 nm) is exhibited by compound ANT-SCH_3 (9-[(*E*)-2-[4-(methylsulfanyl)phenyl]ethenyl]anthracene). This anthracene derivative contains a $-SCH_3$ substituent in its structure, which is classified as an electron-donor. Among the 9-[(*E*)-2-phenylethenyl]phenanthrene derivatives, the following compounds have the most long-wave absorption reaching up to 420 nm: FEN-CN (9-[(*E*)-2-(4-cyanophenyl)ethenyl]phenanthrene), FEN-SCH_3 (9-[(*E*)-2-[4-(methylsulfanyl)phenyl]ethenyl]phenanthrene), FEN-C_6H_5 (9-[(*E*)-2-([1,1′-biphenyl]-4-yl)ethenyl]phenanthrene). The below Table 1 presents the values of molar extinction coefficients of studied chemical compounds at different wavelengths.

Investigation of the electron transfer mechanism between 9-[(*E*)-2 phenylethenyl]anthracene derivatives/9-[(*E*)-2-phenylethenyl]phenanthrene derivatives and the iodonium salt SpeedCure 938

The obtained absorption range of the studied compounds, reaching the visible range, allows supposing that these compounds may find application as photosensitizers in two-component photoinitiating systems, which led to the investigation of the electron transfer mechanism between the components of the initiating system. The study of the mechanism of action of two-component photoinitiating systems was investigated by

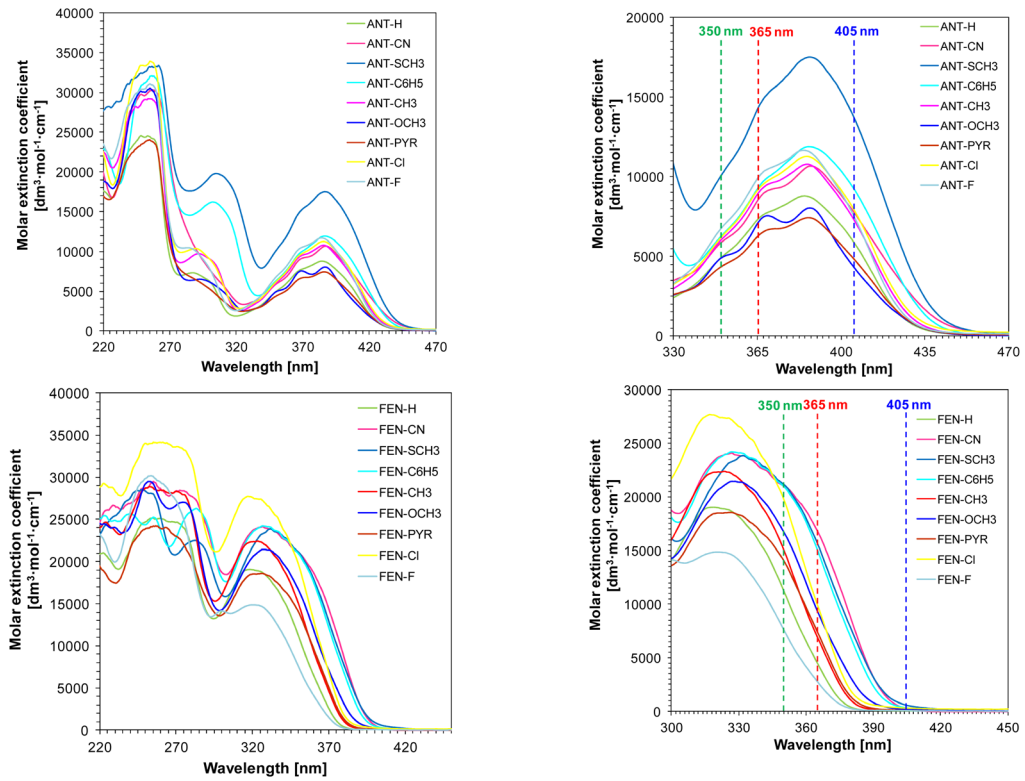

Fig. 3 Absorption spectra of 9-[(*E*)-2-phenylethenyl]anthracene and 9-[(*E*)-2-phenylethenyl]phenanthrene derivatives.

Table 1 Spectroscopic properties of 9-[(*E*)-2-phenylethenyl]anthracene and 9-[(*E*)-2-phenylethenyl]phenantrene derivatives

Acronym	$\lambda_{max\text{-}ab}$ [a] [nm]	$\varepsilon@\lambda_{max\text{-}ab}$ [a]	$\varepsilon@\lambda_{365\ nm}$	$\varepsilon@\lambda_{405\ nm}$	$\varepsilon@\lambda_{420\ nm}$
9-[(*E*)-2-Phenylethenyl]anthracene derivatives					
ANT-H	385	8793	8949	7364	2440
ANT-CN	389	10 667	8354	4368	1742
ANT-SCH_3	389	17 527	14 378	13 593	7426
ANT-C_6H_5	387	11 915	10 886	10 909	5674
ANT-CH_3	386	10 779	8603	5627	1981
ANT-OCH_3	367	8027	9550	4258	1325
ANT-PYR	386	7429	6998	3235	901
ANT-Cl	386	11 270	10 204	8898	3506
ANT-F	384	11 683	7340	5397	1671
9-[(*E*)-2-Phenylethenyl]phenanthrene derivatives					
FEN-H	319	19 057	4293	54	41
FEN-CN	327	24 106	16 633	213	—
FEN-SCH_3	332	23 882	15 434	552	210
FEN-C_6H_5	326	24 913	14 765	305	97
FEN-CH_3	323	22 394	6713	110	89
FEN-OCH_3	327	21 453	9119	206	105
FEN-PYR	326	18 569	7191	90	41
FEN-Cl	317	27 765	9646	270	191
FEN-F	321	14 858	2626	85	54

ε – molar extinction coefficient at λ = 365 nm, λ = 405 nm, λ = 420 nm [$dm^3\ mol^{-1}\ cm^{-1}$]. [a] For the maximum longest wavelength absorption band.

determining the free energy values for the electron transfer process between 9-[(*E*)-2-phenylthenyl]anthracene/9-[(*E*)-2-phenylthenyl]phenanthrene derivatives and the diphenyliodonium salt. The oxidation potential of the tested compounds was determined by cyclic voltammetry in acetonitrile. Based on emission and excitation measurements, which made it possible to determine the energy of singlet states, and based on the determined oxidation potential it was possible to determine the Gibbs free energy. Obtaining negative Gibbs free energy values confirmed the possibility of electron transfer between the 9-[(*E*)-2-phenylethenyl]anthracene/9-[(*E*)-2-phenylethenyl] phenantrene derivatives in the excited state and the iodonium salt in the ground state.

The final step in studying the mechanism was to determine the quantum yield of electron transfer from the excited state. The calculated values of electron transfer quantum yields in the singlet excited state $\Phi_{et(S1)}$ vary from 0.17 to 0.85. It can be seen that phenanthrene derivatives have a higher value of this parameter than its value for analogous derivatives in the anthracene group. All calculated and measured values associated with the electron transfer process are shown in Table 2. The method of calculating each value was shown in the ESI (Fig. S.20–S.107†).

Investigation of the suitability of 9-[(*E*)-2 phenylethenyl] anthracene/9-[(*E*)-2-phenylethenyl]phenanthrene derivatives to the role of photosensitizers of diphenyliodonium salt for initiating the cationic photopolymerization of epoxy monomer CADE

Currently, much attention is paid to the development of cationic photopolymerization technology which is resistant to atmospheric oxygen and during its process there doesn't occur the phenomenon of oxygen inhibition. Thus, cationic photopolymerization processes are particularly interesting and, what is extremely important, they are also relatively widespread in industrial applications because they possess several essential advantages, which determine the practical application of this process. The living nature of cationic photopolymerization ensures that the reaction continues to proceed efficiently even after the radiation source is turned off, a process referred to as dark polymerization. This makes it possible to achieve a high degree of over-reaction, which plays an extremely important role in industrial practice. Therefore, nowadays photoinitiated cationic polymerization plays an increasingly important role as a method to obtain photo-curable polymer coatings.[1,64,65]

First, the suitability of the investigated 9-[(*E*)-2-phenylethenyl]anthracene/9-[(*E*)-2-phenylethenyl]phenanthrene derivatives for the role of iodonium salt photosensitizers to initiate the cationic photopolymerization process of CADE (3,4-epoxycyclohexanecarboxylate 3,4-epoxycyclohexylmethylmethyl) monomer was tested using UV/Vis radiation. The experiments were performed using diodes emitting radiation at wavelengths of λ = 365 nm, λ = 405 nm and λ = 420 nm. The duration of each measurement was 800 s. During the measurement, the epoxy groups present in the CADE monomer structure are lost in favor of the ether bonds formed. This phenomenon is confirmed by: decreasing the intensity of the band at the wavenumber of 790 cm^{-1} (this band corresponds to epoxy groups), increasing the intensity of the band at a wavenumber of 1080 cm^{-1} (this band corresponds to the ether groups).

At first, the photopolymerization process was initiated using a diode emitting radiation of wavelength λ = 365 nm. The obtained epoxy monomer conversions for compositions based on anthracene and phenanthrene derivatives vary between 20 and 62%. The greatest influence on the conversion value was: the molar extinction coefficient of the studied

Table 2 Electrochemical and thermodynamic properties of 9-[(*E*)-2-phenylethenyl]anthracene/9-[(*E*)-2-phenylethenyl]phenantrene derivatives

Compound	$E_{a1/2}$ [mV]	E_{S1} [eV]	$\Delta G_{et(S1)}$ [eV]	$E_{k1/2}$ [mV]	K_{SV} [M^{-1}]	$\Phi_{et(S1)}$	$\tau_{(S1)}$ [ns]	k_q [M^{-1} s^{-1}]
9-[(*E*)-2-Phenylethenyl]anthracene derivatives								
ANT-H	1077	2.90	−1.18	−1790	55.71	0.54	3.41	1.63×10^{10}
ANT-CN	1151	2.79	−1.00	−1578	—	—	—	—
ANT-SCH_3	998	2.81	−1.17	−1773	9.51	0.17	0.81	1.17×10^{10}
ANT-C_6H_5	1053	2.82	−1.13	−1750	51.42	0.52	3.18	1.62×10^{10}
ANT-CH_3	1050	2.88	−1.19	−1813	53.42	0.53	2.64	2.02×10^{10}
ANT-OCH_3	971	2.81	−1.20	−1835	15.36	0.24	—	—
ANT-PYR	1105	2.88	−1.13	−1683	8.13	0.15	—	—
ANT-Cl	1101	3.00	−1.26	−1750	49.43	0.51	3.33	1.48×10^{10}
ANT-F	1078	2.90	−1.18	−1752	43.82	0.48	3.30	1.33×10^{10}
9-[(*E*)-2-Phenylethenyl]phenanthrene derivatives								
FEN-H	1395	3.33	−1.30	−2005	244.53	0.84	1.39	1.76×10^{11}
FEN-CN	1475	3.12	−1.01	−1644	57.38	0.55	0.27	2.13×10^{11}
FEN-SCH_3	1149	3.13	−1.34	−1975	83.65	0.64	0.34	2.46×10^{11}
FEN-C_6H_5	1287	3.19	−1.26	−1933	106.63	0.69	0.81	1.32×10^{11}
FEN-CH_3	1327	3.31	−1.34	−2053	119.79	0.72	0.65	1.84×10^{11}
FEN-OCH_3	1135	3.21	−1.44	−2088	78.71	0.62	—	—
FEN-PYR	1405	3.37	−1.33	−1863	90.60	0.66	0.16	5.66×10^{11}
FEN-Cl	1405	3.29	−1.25	−1915	269.62	0.85	1.27	2.12×10^{11}
FEN-F	1375	3.36	−1.35	−2013	222.01	0.82	0.99	2.24×10^{11}

$E_{a1/2}$ – oxidation potential of photosensitizer [mV]; reference electrode Ag/AgCl. E_{S1} – the singlet state energy of the photosensitizer determined from the excitation and emission spectra. $\Delta G_{et(S1)}$ – Gibbs free energy [eV]. $E_{k1/2}$ – reduction potential [mV]. K_{SV} – Stern–Volmer coefficient [M^{-1}]. $\Phi_{et(S1)}$ – electron transfer quantum yields in the singlet excited state. $\tau_{(S1)}$ – lifetime of the excited state of the sensitizer [ns]. k_q – electron transfer rate constant [M^{-1} s^{-1}]. Electrochemical measurements performed in 0.1 M solution of tetrabutylammonium hexafluorophosphate in acetonitrile; Ag/AgCl reference electrode; Pt working electrode. '—' – not calculated.

anthracene/phenanthrene derivative present in the composition, the value of the oxidation potential, the value of the electron transfer constant between the photosensitizer and the diphenyliodonium salt. Important parameters, which define the efficiency of the two-component initiating systems, are the induction time (time counted from the start of the process until the start of chain growth), the slope of the kinetic curve (tells about the speed of the process occurrence).

Among the compositions based on 9-[(*E*)-2-phenylethenyl] anthracene derivatives, the highest degree of CADE monomer conversion, equal to 62%, was obtained for the sample with compound ANT-SCH_3 (9-[(*E*)-2-[4-(methylsulfanyl)phenyl]ethenyl] anthracene) as the photosensitizer. This compound exhibits a high molar extinction coefficient at 365 nm (11 276 dm^3 mol^{-1} cm^{-1}) and a low oxidation potential (998 mV). High conversion rate (60%) was also obtained for the composition containing compound ANT-C_6H_5 (9-[(*E*)-2-([1,1′-biphenyl]-4-yl)ethenyl]anthracene). Analogous measurements were performed using a diode emitting 405 nm and 420 nm radiation. Monomer conversion values, induction times and kinetic curve slope values for different compositions based on 9-[(*E*)-2-phenylethenyl]anthracene/9-[(*E*)-2-phenylethenyl]phenanthrene derivatives were shown in Table 3.

Under visible light, phenanthrene derivatives do not show suitability as photosensitizers of diphenyliodonium salts to initiate the cationic photopolymerization process. This phenomenon may be due to small values of molar extinction coefficient at wavelength λ = 405 nm and λ = 420 nm.

The obtained results were presented in the ESI (Fig. S.108–S.111†).

Investigation of the suitability of 9-[(*E*)-2 phenylethenyl] anthracene/9-[(*E*)-2-phenylethenyl]phenanthrene derivatives to the role of photosensitizers of diphenyliodonium salt for initiating the radical photopolymerization of acrylate monomer TMPTA

Radical photopolymerization is currently the most widely used method to obtain polymeric materials. The classical radical polymerization process consists of 3 steps: initiation, propagation and termination. One of the factors initiating the polymerization process is light. During the initiation of radical photopolymerization, radicals are formed as a result of the initiator decomposition under ultraviolet or visible radiation.[66–68]

The subsequent research was aimed at verification of the usefulness of the investigated 9-[(*E*)-2-phenylethenyl]anthracene/9-[(*E*)-2-phenylethenyl]phenanthrene derivatives for the role of photosensitizers together with iodonium salt for the initiation of radical photopolymerization of trimethylolpropane triacrylate TMPTA monomer using UV/Vis radiation. Due to the occurrence of oxygen inhibition phenomenon, it was necessary to limit the obviousness of atmospheric oxygen to the photopolymerizing composition. For this purpose, a drop of the composition was applied between two fragments of PP film, thanks to which no negative influence of oxygen on the kinetics of the radical photopolymerization process was observed. The experiments were carried out using light sources in the form of UV/Vis-LEDs emitting radiation with wavelengths of λ = 365 nm, λ = 405 nm and λ = 420 nm, respectively. Then the intensity of the band, which is character-

Table 3 The values of epoxy monomer conversion, kinetic curve slope and induction time were obtained during cationic photopolymerization using UV-Vis LEDs @365 nm, @405 nm, @420 nm

		Cationic polymerization								
		LED @365 nm			LED @405 nm			LED @420 nm		
Acronym		Conversion of CADE monitored at ~790 cm^{-1}	$d\alpha/dt$	Induction time τ_{ind} [s]	Conversion of CADE monitored at ~790 cm^{-1}	$d\alpha/dt$	Induction time τ_{ind} [s]	Conversion of CADE monitored at ~790 cm^{-1}	$d\alpha/dt$	Induction time τ_{ind} [s]
Anthracene derivatives	ANT-H	54	0.20	16.97	41	0.21	6.93	31	0.13	10.14
	ANT-CN	51	0.14	14.87	37	0.28	12.79	27	0.26	3.30
	ANT-SCH_3	62	0.21	21.98	62	0.21	20.19	45	0.31	2.28
	ANT-C_6H_5	60	0.17	13.19	45	0.36	2.20	36	0.14	11.08
	ANT-CH_3	53	0.13	9.29	41	0.26	4.93	28	0.07	11.44
	ANT-OCH_3	58	0.16	21.35	32	0.09	43.74	23	0.28	3.88
	ANT-PYR	49	0.40	2.06	30	0.33	4.16	21	0.14	24.91
	ANT-Cl	59	0.31	8.43	42	0.18	6.04	36	0.20	3.25
	ANT-F	50	0.13	11.77	37	0.12	2.38	25	0.09	5.45
Phenanthrene derivatives	FEN-H	35	0.08	122.04	np	—	—	np	—	—
	FEN-CN	58	0.30	12.31	np	—	—	np	—	—
	FEN-SCH_3	58	0.24	3.73	np	—	—	np	—	—
	FEN-C_6H_5	50	0.12	47.11	np	—	—	np	—	—
	FEN-CH_3	37	0.22	12.79	np	—	—	np	—	—
	FEN-OCH_3	41	0.21	7.70	np	—	—	np	—	—
	FEN-PYR	41	0.09	30.99	np	—	—	np	—	—
	FEN-Cl	50	0.24	10.66	np	—	—	np	—	—
	FEN-F	20	0.04	29.62	np	—	—	np	—	—
REFERENCE		np	—	—	np	—	—	np	—	—

np – no polymerization. Reference = IOD (1% w/w) and CADE without photosensitizers.

istic of the double bonds present in the acrylate monomer was decreased. This band occurs at a wavenumber equal to 1635 cm^{-1}.

Initially, a UV-LED emitting diode with a wavelength of λ = 365 nm was used as the light source. Resulted acrylate monomer conversion rates for compositions based on 9-[(*E*)-2-phenylethenyl]anthracene derivatives as photosensitizers receive 16–36%. The induction times obtained during the measurements for compositions containing 9-[(*E*)-2-phenylethenyl]anthracene derivatives are different. This depended on the type of compound used as a photosensitizer for the diphenyliodonium salt. The shortest induction time (2.32 s) was obtained for the composition with compound ANT-H (9-[(*E*)-2-phenylethenyl]anthracene). For compositions based on 9-[(*E*)-2-phenylethenyl]phenanthrene derivatives, the conversions obtained, during the radical photopolymerization of acrylate monomer TMPTA using a light source emitting ultraviolet radiation, vary between 21 and 54%. The kinetic profile obtained from the composition containing a bimolecular initiating system: iodonium salt and FEN-CN (9-[(*E*)-2-(4-cyanophenyl)ethenyl]phenanthrene) has the conversion rate of 54%.

Analogous measurements were made using light sources emitting radiation in the visible range at @405 nm and @420 nm. All obtained and calculated results are placed in Table 4.

The obtained results were presented in the ESI (Fig. S.112–S.115†).

Investigation of the suitability of 9-[(*E*)-2 phenylethenyl] anthracene derivatives to the role of photosensitizers of diphenyliodonium salt for initiating the hybrid photopolymerization of epoxy and acrylate monomers (CADE/TMPTA/M100)

A modern approach to light-induced polymerization is hybrid polymerization, which combines the advantages of different photopolymerization processes because they combine different polymerization mechanisms or various types of materials. One kind of hybrid photopolymerization is type one polymerization, which uses materials that polymerize according to two different mechanisms: radical and cationic. This process leads to the formation of interpenetrating polymer networks (IPNs). System IPNs is currently attracting a great deal of interest due to their vast potential applications. They can be used *e.g.* as sound and vibration damping materials, in impact-resistant materials, as hardened plastics, membranes. They can find also be used in electrical insulation, coatings, encapsulants and drug carriers.[69–71]

The influence of oxygen on the photopolymerizable composition could be tested by conducting the hybrid photopolymerization process under three different conditions ((1) aerobic conditions, thin layer; (2) anaerobic conditions, thin layer; (3) anaerobic conditions, thick layer). Four 9-[(*E*)-2-phenylethenyl]anthracene derivatives were selected for testing, differentiated by the type of substituent (ANT-SCH_3,

Table 4 The values of acrylate monomer conversion, kinetic curve slope and induction time were obtained during radical photopolymerization using UV-Vis LEDs @365 nm, @405 nm, @420 nm

		Radical polymerization								
		LED @365 nm			LED @405 nm			LED @420 nm		
Acronym		Conversion of TMPTA monitored at ~1635 cm^{-1}	$d\alpha/dt$	Induction time τ_{ind} [s]	Conversion of TMPTA monitored at ~1635 cm^{-1}	$d\alpha/dt$	Induction time τ_{ind} [s]	Conversion of TMPTA monitored at ~1635 cm^{-1}	$d\alpha/dt$	Induction time τ_{ind} [s]
Anthracene derivatives	ANT-H	30	0.22	2.32	27	0.30	7.05	5	0.04	30.28
	ANT-CN	34	0.13	14.34	21	0.21	7.43	23	0.09	7.54
	ANT-SCH_3	36	0.26	8.25	33	0.41	5.65	12	0.08	17.48
	ANT-C_6H_5	34	0.14	2.67	32	0.33	13.65	14	0.10	2.27
	ANT-CH_3	32	0.27	11.03	25	0.28	11.70	13	0.08	14.86
	ANT-OCH_3	36	0.22	18.95	19	0.19	15.58	11	0.09	9.01
	ANT-PYR	16	0.05	23.50	12	0.05	23.50	9	0.04	19.55
	ANT-Cl	32	0.21	10.59	32	0.15	13.98	11	0.07	1.78
	ANT-F	21	0.09	3.77	23	0.22	14.25	5	0.03	18.69
Phenanthrene derivatives	FEN-H	32	0.07	2.47	np	—	—	np	—	—
	FEN-CN	54	0.49	34.46	17	0.09	31.15	np	—	—
	FEN-SCH_3	50	0.36	36.79	21	0.18	14.32	10	0.05	18.71
	FEN-C_6H_5	47	0.15	10.55	18	0.07	32.19	np	—	—
	FEN-CH_3	34	0.14	2.68	np	—	—	np	—	—
	FEN-OCH_3	40	0.10	4.04	5	0.03	8.21	np	—	—
	FEN-PYR	39	0.17	79.76	np	—	—	np	—	—
	FEN-Cl	47	0.17	37.04	np	—	—	np	—	—
	FEN-F	21	0.09	3.77	np	—	—	np	—	—
REFERENCE		np	—	—	np	—	—	np	—	—

np – no polymerization. Reference = IOD (1% w/w) and TMPTA without photosensitizers.

ANT-C_6H_5, ANT-CH_3, ANT-Cl). The initiating system (anthracene derivative/IOD (0.1/1% by weight)) was dissolved in the monomer mixture (CADE/TMPTA/M100: 2/2/1). The following Fig. 4 show the conversion rates of epoxy and acrylate groups during measurements for which a diode emitting radiation at a wavelength of 405 nm as the light source was used.

In the case when anaerobic conditions were used, for both thin and thick films, higher conversion rates were obtained for acrylate groupings (Fig. 4a and c and Fig. S.116†). On the other hand, when oxygen conditions were used, higher conversion rates were obtained for epoxy groups (Fig. 4b). This unequivocally demonstrates the fact that oxygen inhibition occurs in radical photopolymerization, which is disordered in photo-curable 3D printing. Thus, when designing resin formulations for 3D printing, the unfavorable effect of oxygen inhibition must be taken into account. Nevertheless, the process of radical photopolymerization with newly developed photoinitiating systems does occur – but the conversion rates achieved are lower than when using laminates (Table 5).

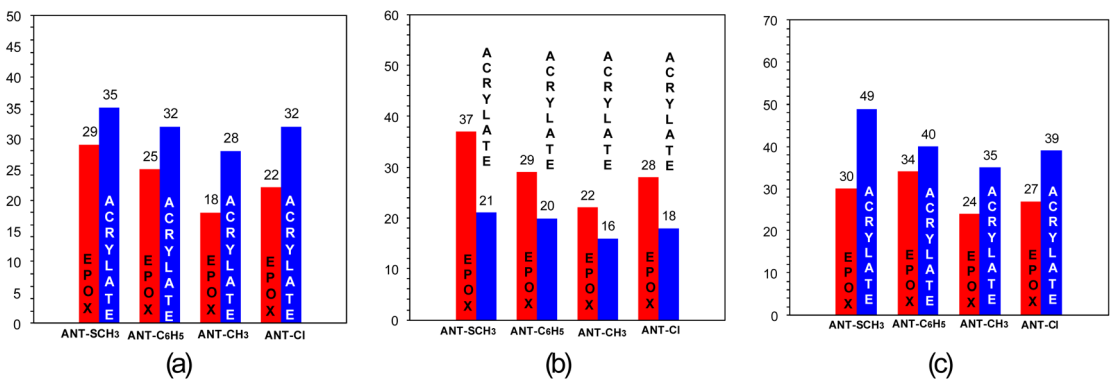

Fig. 4 Acrylate and epoxy monomer conversions obtained during hybrid photopolymerization of CADE/TMPTA/M100 monomers for bimolecular photoinitiating systems based on various 9-[(*E*)-2-phenyl]anthracene derivatives (ANT-SCH_3, ANT-C_6H_5, ANT-CH_3, ANT-Cl) and iodonium salt SpeedCure 938; radiation source – a diode emitting radiation at a wavelength of 405 nm (a) laminate condition, thin layer; (b) air thin layer; (c) laminate condition, thick layer.

Table 5 The values of acrylate and epoxy monomer conversion were obtained during hybrid photopolymerization using Vis LED @405 nm during different experimental conditions

Light source: LED @405 nm							
				Functional group conversion			
Composition	Experimental conditions	Thickness	Monitoring wavelengths	ANT-SCH_3	ANT-C_6H_5	ANT-CH_3	ANT-Cl
CADE/TMPTA/M100 (2/2/1 w/w/w)	Laminate	25 μm	EPOX at 790 cm^{-1}	29	25	18	22
			ACRYLATE at 1.635 cm^{-1}	35	32	28	32
	Air thin layer	25 μm	EPOX at 790 cm^{-1}	37	29	22	28
			ACRYLATE at 1.635 cm^{-1}	21	20	16	18
	Air thick layer	1.16 mm	EPOX at 3.700 cm^{-1}	30	34	24	27
			ACRYLATE at 6.165 cm^{-1}	49	40	35	39

Investigation of the suitability of 9-[(*E*)-2 phenylethenyl] anthracene derivative (ANT-CH_3) to the role of photosensitizers of diphenyliodonium salt for initiating the hybrid photopolymerization of acrylate monomers (HEMA/BEDA) in the presence of various nanofillers

In the next step, experiments were conducted with new initiating system and two different monomers: bisphenol A ethoxylate diacrylate (BEDA) and 2-hydroxyethyl methacrylate (HEMA) (7/3 w/w) that polymerize according to the same mechanism: radical photopolymerization For this research, the most effective initiating system to date has been selected in the form of the ANT-CH_3 (0.1% by weight), SpeedCure 938 diphenyliodonium salt (1% by weight). In addition, various nanoparticles (as nanosubstituents) were added to the above composition in subsequent steps to test their effect on photopolymerization kinetics. The experiments were conducted on rings (thick layers) to avoid the negative influence of oxygen on the photopolymerizing composition. The experiments were conducted using a high power diode emitting radiation at @405 nm. The conducted tests showed that the addition of the studied nanoparticles didn't show accelerating and sensitizing properties, but also didn't show inhibitory properties. The quantity of added nanoparticles was optimized accordingly, the amounts of nanoparticles were selected so as not to cause interference on the FT-IR spectrum, as well as during 3D printing. For instance, halloysite nanoclay does not absorb radiation, which makes it possible to add it in large amounts to a photo-curable formulation, which is why it was decided to add it at 3% by weight. However, the titanium oxide nanoadditive caused interference on the FT-IR spectrum (saturation of the band characteristic of C=C double bonds), so it was decided to add it in an amount of 0.1% by weight. As can be seen from the described example, the addition of each type of nanoparticle requires appropriate optimization.[72]

To achieve even higher conversion rates, it was decided to test a three-component system formulated as ANT-CH_3, IOD (0.1/1 w/w) and 3% *N*-methyldiethanolamine (MDEA). The photopolymerization process was carried out under the same conditions as when the binary system was employed. It can then be clearly seen that the amine accelerates the radical photopolymerization of HEMA/BEDA monomers, with conversion rates reaching almost 100%, which is extremely important in 3D printing.

The following Table 6 and Fig. S.117 and S.118 in the ESI† present the results obtained during hybrid photopolymerization.

Determination of optimum printing parameters – Jacob working curves

The next stage of the research was to determine the optimal printing parameters (E_0 and C_d) for compositions selected for 3D printing tests. Determining the curing time of the layer is highly significant, as too short a time can result in the resin being uncured, while too long a time can result in the resin

Table 6 The values of acrylate monomer conversion were obtained during hybrid radical photopolymerization using Vis LED @405 nm

Light source: LED @405 nm									
					Functional group conversion				
Composition	Experimental conditions	Thickness	Monitoring wavelengths	Light intensity [mW cm^{-2}]	ANT-CH_3 (without nanofiller)	ANT-CH_3, 1% w/w AlZnO	ANT-CH_3, 1% w/w ZnO	ANT-CH_3, 3% w/w halloysite nanoclay	ANT-CH_3, 0.1% w/w TiO_2
HEMA/BEDA (3/7 w/w), 3% MDEA, 1% IOD	Thick layer	1.16 mm	ACRYLATE at 6165 cm^{-1}	26.50	96	95	86	94	94
				2.65	29	33	21	42	28
HEMA/BEDA (3/7 w/w), 1% IOD				26.50	68	56	63	71	88
				2.65	26	26	12	15	12

being cured throughout the bath and not just the desired object. Correctly defining printing parameters is extremely important as it affects the quality, and thus the resolution of the obtained printout. Determining the critical energy defines the minimum energy needed to crosslink the light-curing resin. To determine the relevant printing parameters it is necessary to apply the Jacob test. Jacob's test was performed for the following light-curing compositions containing HEMA/BEDA (3/7 w/w) monomers: (1) ANT-CH_3, IOD (0.1/1 w/w), 3% MDEA; (2) ANT-CH_3, IOD (0.1/1 w/w), 3% MDEA, 0.1% TiO_2; (3) ANT-CH_3, IOD (0.1/1 w/w), 3% MDEA, 1% ZnO; (4) ANT-CH_3, IOD (0.1/1 w/w), 3% MDEA, 1% AlZnO; (5) ANT-CH_3, IOD (0.1/1 w/w), 3% MDEA, 3% halloysite nanoclay. To determine the printing parameters for the resin, slices with design dimensions of 1 × 1 × 0.3 mm were printed, the exposure time of the samples varied from 120 s to 600 s. The print thickness (C_d) was then measured using a screw micrometer and the thickness measurements were repeated 5 times for each sample. Fig. 5 shows a comparison of the results obtained for the resin: ANT-CH_3 + IOD (0.1/1 w/w) + 3% MDEA + HEMA/BEDA (3/7) with the corresponding nano-additives using the Jacob's working curve method.

From the above plot of $C_d = f(E_0)$, the equations were obtained, from which the critical energy values were determined for each of the photo-curable resins. The Table 7 below presents the calculated critical energy values.

Based on the results obtained, it can be concluded that the use of nano-additives such as ZnO or AlZnO allows for a significant reduction of the critical energy values, which in subsequent studies can be translated into shorter printing times.

Application of anthracene derivatives in additive manufacturing using light-initiated techniques

Radical polymerization. The application tests were then carried out – 3D printing using the new initiating system containing the most effective photosensitizer ANT-CH_3. In the first stage, a laser engraver was used for 3D printing tests (direct ink writing technology). The method using an engrav-

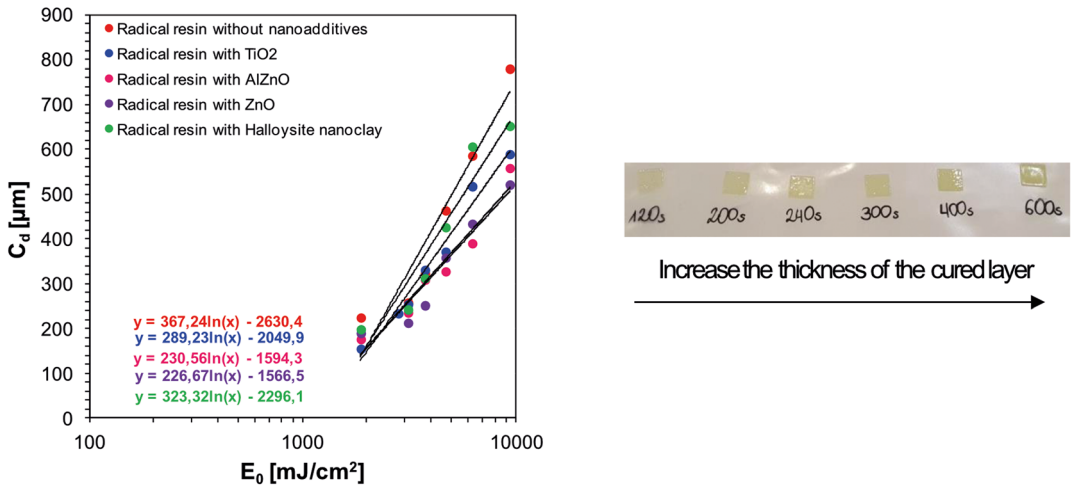

Fig. 5 Determination of optimal printing parameters for a photo-curable resin: ANT-CH_3 + IOD (0.1/1 w/w) + 3% MDEA + HEMA/BEDA (3/7) without nano additives and with TiO_2, AlZnO, ZnO and halloysite nanoclay; slices printed from ANT-CH_3 + IOD composition (0.1/1 w/w) + 3% MDEA + HEMA/BEDA (3/7) for Jacob's test.

Table 7 Critical energy value and curing light penetration depth for radical resins with different nano-additives based on Jacob's test

Radical resin	Equation	Critical energy [mJ cm^{-2}]	Critical energy [%] (in relation to formulation without nanoadditives)	Curing light penetration depth [µm]	Curing light penetration depth [%] (in relation to formulation without nanoadditives)
Without nanoadditives	$y = 367.24 \ln(x) - 2630.4$	1290.29	100	318	100
With TiO_2	$y = 289.23 \ln(x) - 2049.9$	1196.84	93	265	83
With AlZnO	$y = 230.56 \ln(x) - 1594.3$	1007.17	78	235	74
With ZnO	$y = 226.67 \ln(x) - 1566.5$	1003.18	78	191	60
With halloysite nanoclay	$y = 323.32 \ln(x) - 2296.1$	1213.95	94	277	87

ing machine involves curing a liquid resin with a laser that emits radiation in the visible range. The additive manufacturing process is carried out layer by layer. For these experiments, photo-curable resins with an initiator system based on 9-[(*E*)-2-phenylethenyl]anthracene derivatives and iodonium salt (0.1/1 w/w) were used, while the monomer composition was as follows: CADE/TMPTA/M100 (2/2/1). Printouts were obtained at a light intensity of 1500 mW cm^{-2} and a wavelength of λ = 405 nm (spot size 0.075 mm). Each printout obtained consists of 4 layers. The curing time for the first layer was about 40 s and for each subsequent layer about 30 s. The graphic below illustrates images of the print obtained from one of the compositions based on the anthracene derivative ANT-CH_3 (Fig. 6).

Photographs of prints obtained from the other compositions based on 9-[(*E*)-2-phenylethenyl]anthracene derivatives were presented in the ESI (Photo 1†).

The next research step was to investigate 3D printing using DLP technology. For this purpose, the Anycubic Photon Mono X printer was used. Three types of light-curing compositions were applied for testing: (1) radical composition: ANT-CH_3, IOD (0.1/1 w/w), 3% MDEA, HEMA/BEDA (3/7); (2) radical composition with nano-additive ANT-CH_3, IOD (0.1/1 w/w), 3% MDEA, HEMA/BEDA (3/7), 0.1% TiO_2; (3) hybrid composition ANT-SCH_3, IOD (0.1/1 w/w), 3% MDEA, CADE/TMPTA/M100 (2/2/1). The first composition to be tested for 3D printing was a basic radical composition. Based on Jacob's test, the exposure time of one layer was selected, the irradiation time was 160 s. The project of a 1 × 1 × 1 cube was created in Autodesk Fusion 360. The total printing time was 284 minutes, with an exposure time of 300 seconds for the three bottom layers and 160 seconds for each subsequent layer. The following Fig. 7 shows pictures of the individual faces of the cube. In this case, the cube with very good resolution was obtained.

In turn, it was decided to test how the addition of TiO_2 (0.1% by weight) to the composition: ANT-CH_3, IOD (0.1/1 w/w), 3% MDEA, HEMA/BEDA (3/7) would affect the quality of the resulting print and whether any problems would arise during the process, such as particles of the nano-additive falling to the bottom of the bath. Based on the results obtained with Jacob working curves, it was found that the exposure time for a single layer can be slightly shorter than for the same resin but without TiO_2. Therefore, the exposure time for the three initial layers was 300 s, while each subsequent layer was 150 s, which reduced the printing time (the total process time was 268 min). The quality of the resulting print is very high, as can be seen from the resolution of the elements on the individual faces of the cube. During the printing process, no problems caused by the presence of titanium oxide in the tested composition were noticed (Fig. 8a).

Moreover SEM analysis showed the presence of regular patterns on the sample surface after 3D printing (Fig. 8b). These patterns are diamond-shaped and evenly distributed over the sample surface. The layers of material formed during the printing process are also visible. No cracks or surface defects were observed which proves the high quality of the prints. In addition, based on the resulting images, you can determine the accuracy of the Anycubic Photon Mono X printer, which is 50 μm.

Hybrid polymerization

The last resin made for 3D printing testing, was a hybrid resin: ANT-SCH_3, IOD (0.1/1 w/w), 3% MDEA, CADE/TMPTA/M100 (2/2/1). During the kinetic measurements, quite high conversion rates of both epoxy and acrylate groups were observed, yet some problems appeared during printing. At first, an attempt was made to print a 1 × 1 × 1 cm cube. The exposure time for the three initial layers was 300 s, while each subsequent layer was 150 s. A photograph of one of the cube walls is shown in Fig. 9a.

The first few layers (about 30 layers) of the above print have good resolution, as can be seen from observing the resulting cube. However, each successive layer is cross-linked, not only the exposed area but also the area around the print is cured. This may be due to the fact that a hybrid resin (epoxy and acrylate monomers) is involved, the process shows characteristics of cationic and radical photopolymerization. As mentioned earlier, one of the features of cationic photopolymerization is that it occurs even when the light source is switched off. This is also the case with this print. Photopolymerization occurs effectively not only when the desired area is irradiated, but also when the light source is not switched on so that cross-linking occurs throughout the bath. The total printing time for this cube was 268 min, a time that is too long for this hybrid resin. A solution to this problem with cross-linking of the

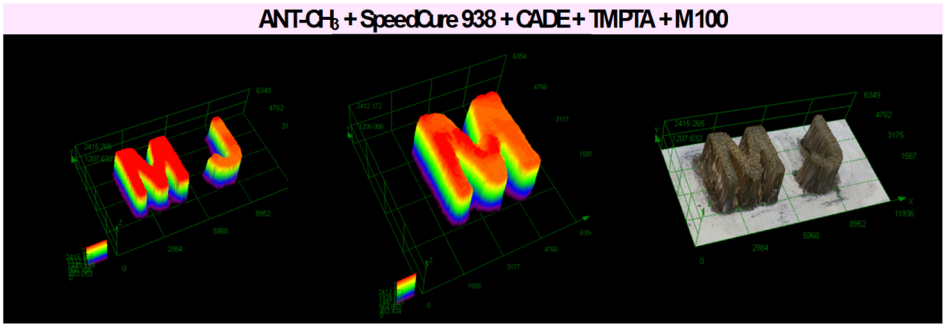

Fig. 6 Photographs of a 3D printout obtained from a hybrid composition based on ANT-CH_3 compound.

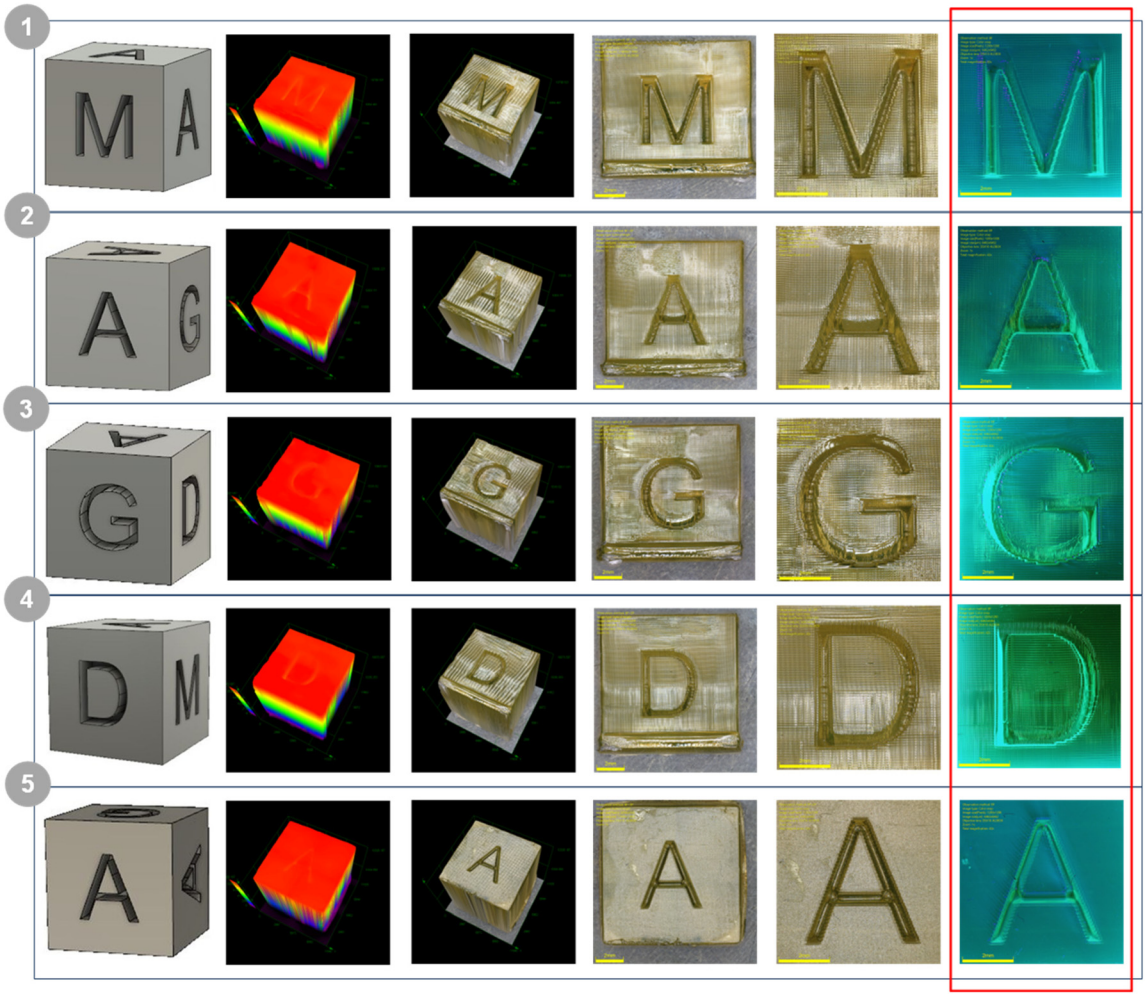

Fig. 7 Photographs of a printout obtained from a photo-cured resin: ANT-CH_3, IOD (0.1/1 w/w), 3% MDEA, HEMA/BEDA (3/7) (1–5 individual faces of a cube with different letters); last column – photographs were taken under the UV flashlight.

resin in the entire volume of the bathtub could be shortened. However the reduction in time must not be too drastic, as this may result in the individual layers of the print not curing.

Considering the above a second attempt was made to obtain a print from a hybrid composition (CADE/TMPTA/M100). For this purpose, the printing parameters of the same cube were modified in special software. These modifications were aimed at reducing the total exposure time of the resin. The curing time of the initial three layers was 300 s. The next 10 layers were transition layers, indicating that the time of each successive layer of these 10 decreased linearly from a value of 300 s to 100 s. All other layers were exposed at 100 s (each layer). This treatment reduced the total printing time, which was 185 minutes. Unfortunately, it turned out that the exposure time for the initial layers (about 10 layers) was altogether too long, causing the cross-linked resin to stick to the bottom of the bath and the print to fail, as shown in Fig. 9b.

A third attempt was made to obtain a print from a hybrid composition (CADE/TMPTA/M100). For this purpose, a 1 × 1 × 0.5 cm printout has been drawn up. Reducing the cube height allowed for shorter printing times. Fig. 9c shows the individual walls of the resulting print. Reducing the printing time allowed to obtain a three-dimensional object with good resolution, without over-polymerized layers.

Reducing the print height does not solve the problem that occurs when printing with hybrid resin. A solution to this problem could be to set different exposure times for the individual print layers. It is therefore necessary to make changes to the 3D printer software, as at the moment you can only set two different times, one is the exposure time for the bottom layer (or several bottom layers), while the other time is the exposure time for each subsequent layer.

Another attempt to obtain a printout from a hybrid composition (CADE/TMPTA/M100) consisted in modification of the initiating system, from which it was decided to exclude the amine MDEA, thus the photoinitiating system contained ANT-SCH_3/IOD (0.1/1% by weight). The addition of MDEA amine to the photocurable resin allows to significantly accelerate the process of obtaining photocurable composites. In the case of a hybrid formulation containing monomers polymerizing according to the radical and cationic mechanism, the

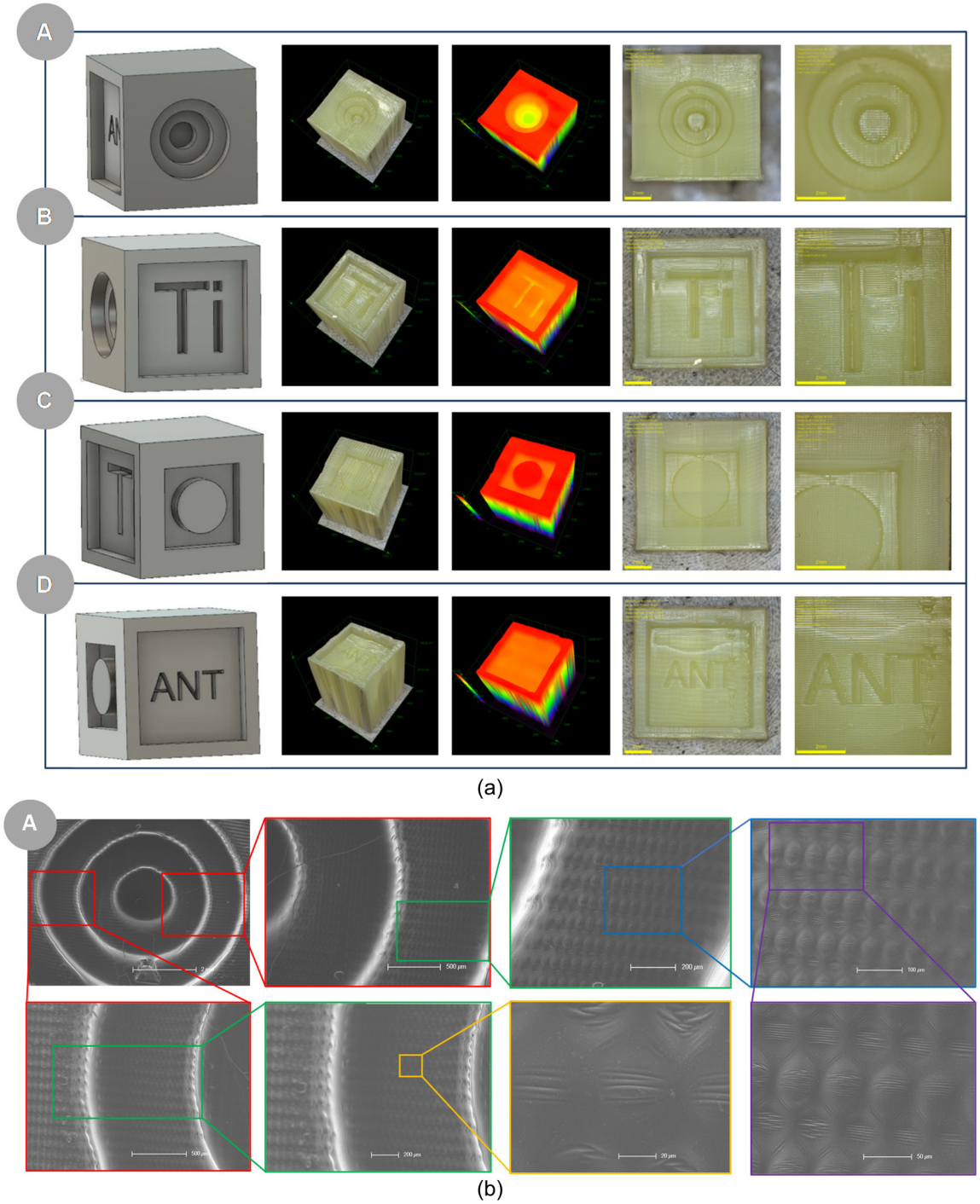

Fig. 8 Photographs of a printout obtained from a photo-cured resin: ANT-CH_3, IOD (0.1/1 w/w), 3% MDEA, HEMA/BEDA (3/7), 0.1% TiO_2 (A–D individual faces of a cube with different letters): (a) under an optical microscope, (b) under a scanning electron microscope.

addition of MDEA caused the resin to overheat, which affected the resin's over-polymerization, resulting in very poor quality of the resulting print. The elimination of MDEA amine from the resin formulation eliminated the problem of resin overheating and optimized the printing parameters of the hybrid resin, thus resulting in longer printing times. The photograph below shows the results obtained.

Eliminating amine from the composition of the hybrid resin avoided the effect of excessive polymerization during the printing process. The resulting print is characterized by high resolution (Fig. 10).

The final stage of the study was an attempt to print a nanocomposite from the photo-curable composition ANT-SCH_3, IOD (0.1/1 w/w), CADE/TMPTA/M100 with titanium oxide

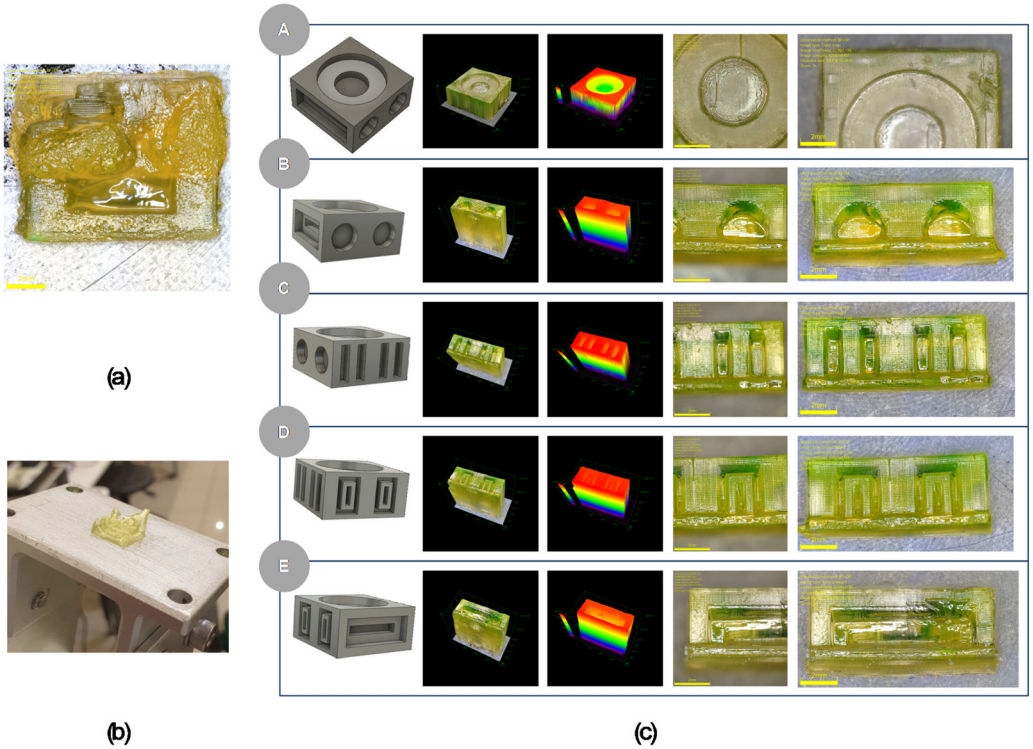

Fig. 9 Photographs of prints obtained from a photo-cured resin: ANT-SCH_3, IOD (0.1/1 w/w), 3% MDEA, CADE/TMPTA/M100 (2/2/1). (a) First attempt, (b) second attempt, (c) third attempt.

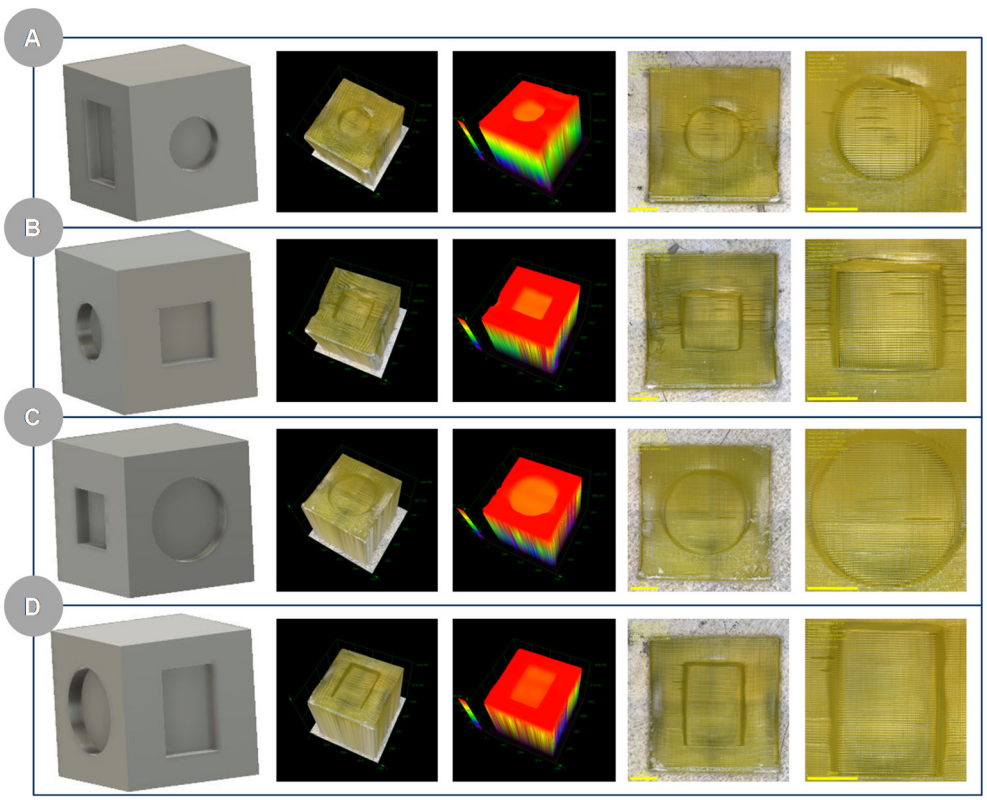

Fig. 10 Photographs of a printout obtained from a photo-cured resin: ANT-SCH_3, IOD (0.1/1 w/w), CADE/TMPTA/M100 (2/2/1) (A–D individual faces of a cube).

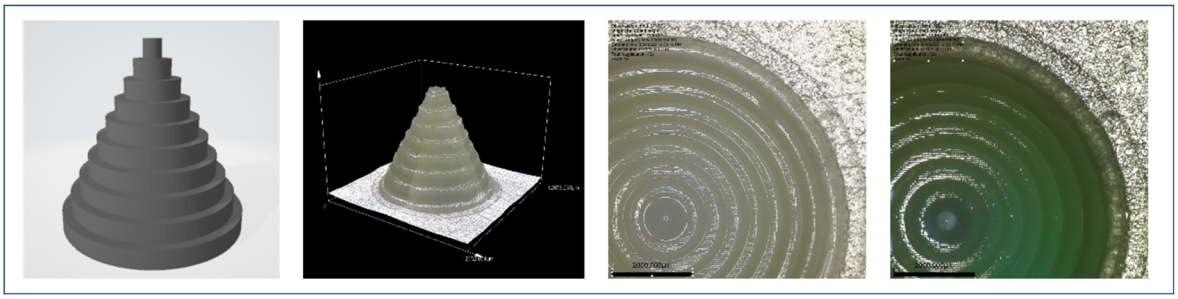

Fig. 11 Photographs of a printout obtained from a photo-cured resin: ANT-SCH_3, IOD (0.1/1 w/w), CADE/TMPTA/M100 (2/2/1), 0.1% TiO_2.

Table 8 3D printing parameters for photo-cured resins

Composition	Number of bottom layers	Exposure time of bottom layers [s]	Exposure time of individual layers [s]	Layer height [mm]	Print time [min]	Print size [cm × cm × cm]	Print
ANT-CH_3, IOD (0.1/1 w/w), 3% MDEA, HEMA/BEDA (3/7)	3	300	160	0.1	284	1 × 1 × 1	✓
ANT-CH_3, IOD (0.1/1 w/w), 3% MDEA, HEMA/BEDA (3/7), 0.1% TiO_2	3	300	150	0.1	268	1 × 1 × 1	✓
ANT-SCH_3, IOD (0.1/1 w/w), 3%	3	300	150	0.1	138	1 × 1 × 0.5	✓
MDEA, CADE/TMPTA/M100 (2/2/1)	3	300	150	0.1	268	1 × 1 × 1	◀
ANT-SCH_3, IOD (0.1/1 w/w), CADE/TMPTA/M100 (2/2/1)	3	300	170	0.1	300	1 × 1 × 1	✓
ANT-SCH_3, IOD (0.1/1 w/w), CADE/TMPTA/M100 (2/2/1), 0.1% TiO_2	3	300	160	0.1	284	1 × 1 × 1	✓

added. In this case, the printout with very good resolution was obtained (Fig. 11).

The printing parameters of all the formulations discussed are summarized in Table 8.

Conclusions

Nowadays, 3D printing plays an extremely important role in creating three-dimensional objects for various applications. More and more frequently, 3D printing techniques can be found where photo-cured resins are used as input material, so it is very important to constantly improve photoinitiating systems, as well as the monomer composition of resins. In this paper, the suitability of 9 compounds from the anthracene group, as well as 9 compounds from the phenanthrene group, varied in terms of the type of attached substituent to act as photosensitizers of iodonium salts, was investigated. The examined initiator systems showed versatile performance, and can be successfully applied as photoinitiators for radical, cationic and hybrid photopolymerization. The innovative application of the new high-performance initiator systems is their usage for obtaining photo-curable nanocomposites from radical resins, as well as hybrid resins, which has been confirmed by kinetic studies, as well as DLP 3D printing experiments using low-cost equipment. The research studied the effects of different nanoparticles on the kinetic parameters of photo-curable resins, as well as on 3D printing parameters (such as critical energy, for example). Based on several measurements, it was found that the amount of each nano-additive needs to be optimized. The selection of the right amount of nano-additive, resin composition, as well as 3D printing parameters is essential for the correct printing process of nanocomposites, as well as for obtaining a print with high quality and very good resolution. Nevertheless, the above article proves that new initiating systems based on anthracene derivatives are useful for obtaining prints from commonly used monomers that polymerize according to the radical mechanism. However, the novelty is also that they can initiate the process of hybrid photopolymerization. As a result, allergenic monomers polymerizing according to the radical mechanism have been reduced in the formulation. This is a precursor for the development of new hybrid formulations and opens the way to formulations polymerizing only by the cationic mechanism, which is characterized by low polymerization shrinkage.

Conflicts of interest

There are no conflicts to declare.

Note added after first publication

This article replaces the version published on 11 April 2023 which was missing funding information in the Acknowledgements section.

Acknowledgements

The present work was funded by the OPUS LAP project contract number 2020/39/I/ST5/03556 "Advanced photopolymerized nanocomposite materials processed by additive manufacturing". M.P. is grateful for financial support from the project "ROAD TO EXCELLENCE - a comprehensive university support programme" implemented under the Operational Programme Knowledge Education Development 2014–2020 co-financed by the European Social Fund; agreement no. POWR.03.05.00-00-Z214/18 (The National Centre for Research and Development). One of the authors M.T.S. would like to thank Foundation for Polish Science (Warsaw, Poland), project START, Grant No. START 088.2023.

References

1 L. Pierau, C. Elian, J. Akimoto, Y. Ito, S. Caillol and D. L. Versace, *Prog. Polym. Sci.*, 2022, **127**, 101517.
2 M. Topa, J. Ortyl, A. Chachaj-Brekiesz, I. Kamińska-Borek, M. Pilch and R. Popielarz, *Spectrochim. Acta, Part A*, 2018, **199**, 430–440.
3 I. V. Khudyakov, *Prog. Org. Coat.*, 2018, **121**, 151–159.
4 B. Bao, J. You, D. Li, H. Zhan, L. Zhang, M. Li and T. Wang, *J. Photochem. Photobiol., A*, 2022, **429**, 113938.
5 I. Chiulan, E. B. Heggset, Ș. I. Voicu and G. Chinga-Carrasco, *Biomacromolecules*, 2021, **22**, 1795–1814.
6 E. Nicol, *Biomacromolecules*, 2021, **22**, 1325–1345.
7 A. Al Rashid, W. Ahmed, M. Y. Khalid and M. Koç, *Addit. Manuf.*, 2021, **47**, 102279.
8 W. Tomal and J. Ortyl, *Polymers*, 2020, **12**, 1073.
9 W. Tomal, D. Krok, A. Chachaj-Brekiesz and J. Ortyl, *Eur. Polym. J.*, 2021, **156**, 110603.
10 F. Zhang, L. Zhu, Z. Li, S. Wang, J. Shi, W. Tang, N. Li and J. Yang, *Addit. Manuf.*, 2021, **48**, 102423.
11 S. Liu, Y. Zhang, K. Sun, B. Graff, P. Xiao, F. Dumur and J. Lalevée, *Eur. Polym. J.*, 2021, **147**, 2021.
12 A. Al Rashid, W. Ahmed, M. Y. Khalid and M. Koç, *Addit. Manuf.*, 2021, **47**, 102279.
13 E. Hola, M. Pilch, M. Galek and J. Ortyl, *Polym. Chem.*, 2020, **11**, 480–495.
14 W. Tomal, T. Świergosz, M. Pilch, W. Kasprzyk and J. Ortyl, *Polym. Chem.*, 2021, **12**, 3661–3676.
15 M. Topa and J. Ortyl, *Materials*, 2020, **13**, 4093.
16 S. Asif, P. Chansoria and R. Shirwaiker, *J. Manuf. Process.*, 2020, **56**, 1340–1343.
17 I. Kim, S. Kim, A. Andreu, J. H. Kim and Y. J. Yoon, *Addit. Manuf.*, 2022, **52**, 102659.
18 H. Wu, W. Liu, L. Lin, Z. Huang, S. Wei, S. Wu, Z. Sun, D. An and Z. Xie, *Mater. Chem. Phys.*, 2022, **285**, 126090.
19 M. Štaffová, F. Ondreáš, J. Svatík, M. Zbončák, J. Jančář and P. Lepcio, *Polym. Test.*, 2022, **108**, 107499.
20 J. Li, S. Li, Y. Li, R. Li, J. Nie and X. Zhu, *J. Photochem. Photobiol., A*, 2020, **389**, 112225.
21 A. Andreu, P. C. Su, J. H. Kim, C. Siang, S. Kim, I. Kim, J. Lee, J. Noh, A. Suriya and Y. J. Yoon, *Addit. Manuf.*, 2021, **44**, 102024.
22 E. Hola, M. Topa, A. Chachaj-Brekiesz, M. Pilch, P. Fiedor, M. Galek and J. Ortyl, *RSC Adv.*, 2020, **10**, 7509–7522.
23 P. Fiedor, M. Pilch, P. Szymaszek, A. Chachaj-Brekiesz, M. Galek and J. Ortyl, *Catalysts*, 2020, **10**, 284.
24 W. Tomal, D. Krok, A. Chachaj-Brekiesz, P. Lepcio and J. Ortyl, *Addit. Manuf.*, 2021, **48**, 102447.
25 J. Segurola, N. S. Allen, M. Edge, A. McMahon and S. Wilson, *Polym. Degrad. Stab.*, 1999, **64**, 39–48.
26 M. Topa, E. Hola, M. Galek, F. Petko, M. Pilch, R. Popielarz, F. Morlet-Savary, B. Graff, J. Laleveé and J. Ortyl, *Polym. Chem.*, 2020, **11**, 5261–5278.
27 J. Ortyl, M. Topa, I. Kamińska-Borek and R. Popielarz, *Eur. Polym. J.*, 2019, **116**, 45–55.
28 M. Topa and J. Ortyl, *J. Photopolym. Sci. Technol.*, 2021, **34**, 259–262.
29 E. Hola and J. Ortyl, *Eur. Polym. J.*, 2021, **150**, 110365.
30 J. Ortyl, M. Galek, P. Milart and R. Popielarz, *Polym. Test.*, 2012, **31**, 466–473.
31 H. F. Gruber, *Prog. Polym. Sci.*, 1992, **17**, 953–1044.
32 L. Breloy, C. Negrell, A. S. Mora, W. S. J. Li, V. Brezová, S. Caillol and D. L. Versace, *Eur. Polym. J.*, 2020, **132**, 109727.
33 M. Yao, S. Liu, C. Huang, J. Nie and Y. He, *J. Photochem. Photobiol., A*, 2021, **419**, 113451.
34 G. S. Batibay, O. T. Gunkara, N. Ocal and N. Arsu, *Prog. Org. Coat.*, 2020, **149**, 105939.
35 J. P. Fouassier, D. Ruhlrnann, K. Zahouily, E. Nationale, L. Angiolini, C. Carlini and N. Lelli, *Polymer*, 1992, **33**, 3569–3573.
36 L. Angiolini, D. Caretti, C. Carlini, E. Corelli and P. A. Rolla, *Polymer*, 1994, **35**, 5413–5421.
37 Y. Wu, R. Li, C. Huang, J. Wu, X. Sun and Y. Situ, *Prog. Org. Coat.*, 2022, **168**, 106876.
38 G. Xie, Z. Shuai, Y. Huang, M. Yu, Z. Zeng and J. Yang, *Prog. Org. Coat.*, 2020, **147**, 105716.
39 J. E. Baxter, R. S. Davidson and H. J. Hageman, *Eur. Polym. J.*, 1988, **24**, 551–556.
40 N. Karaca, G. Temel, D. K. Balta, M. Aydin and N. Arsu, *J. Photochem. Photobiol., A*, 2010, **209**, 1–6.
41 S. Huo, H. Y. Zhou and J. X. Wang, *React. Funct. Polym.*, 2021, **163**, 104892.
42 G. Ye, Z. Ke, J. Yang, T. Zhao, Z. Zeng and Y. Chen, *Polymer*, 2006, **47**, 4603–4612.
43 T. Xue, Y. Li, X. Zhao, J. Nie and X. Zhu, *Prog. Org. Coat.*, 2021, **157**, 106329.
44 K. Wang, K. Yang and Q. Yu, *Prog. Org. Coat.*, 2014, **77**, 1929–1934.
45 A. Mau, T. H. Le, C. Dietlin, T. T. Bui, B. Graff, F. Dumur, F. Goubard and J. Lalevee, *Polym. Chem.*, 2020, **11**, 7221–7234.
46 E. Metin, N. Arsu, S. Catak and V. Aviyente, *Eur. Polym. J.*, 2020, **136**, 109909.

47 S. K. Doğruyol, Z. Doğruyol and N. Arsu, *J. Lumin.*, 2013, **138**, 98–104.
48 E. Hola, P. Fiedor, A. Dzienia and J. Ortyl, *ACS Appl. Polym. Mater.*, 2021, **3**, 5547–5558.
49 L. M. Barcelos, M. G. Borges, C. J. Soares, M. S. Menezes, V. Huynh, M. G. Logan, A. P. P. Fugolin and C. S. Pfeifer, *Dent. Mater.*, 2020, **36**, 468–477.
50 A. F. Lima, M. V. O. Salvador, D. Dressano, C. H. C. Saraceni, L. S. Gonçalves, M. Hadis and W. M. Palin, *J. Mech. Behav. Biomed. Mater.*, 2019, **98**, 71–78.
51 J. Ortyl, J. Wilamowski, P. Milart, M. Galek and R. Popielarz, *Polym. Test.*, 2015, **48**, 151–159.
52 A. Al Mousawi, C. Dietlin, B. Graff, F. Morlet-Savary, J. Toufaily, T. Hamieh, J. P. Fouassier, A. Chachaj-Brekiesz, J. Ortyl and J. Lalevée, *Macromol. Chem. Phys.*, 2016, **217**, 1955–1965.
53 E. Hola, J. Ortyl, M. Jankowska, M. Pilch, M. Galek, F. Morlet-Savary, B. Graff, C. Dietlin and J. Lalevée, *Polym. Chem.*, 2020, **11**, 922–935.
54 P. Xiao, F. Dumur, B. Graff, F. Morlet-Savary, D. Gigmes, J. P. Fouassier and J. Lalevée, *Macromolecules*, 2014, **47**, 973–978.
55 K. Sun, C. Pigot, H. Chen, N. Malek, D. Gigimes, F. Morlet-Savary, B. Graff, S. Liu, P. Xiao, F. Dumur and J. Lalevée, *Catalysts*, 2020, **10**, 463.
56 S. Liu, Y. Zhang, K. Sun, B. Graff, P. Xiao, F. Dumur and J. Lalevée, *Eur. Polym. J.*, 2021, **147**, 110300.
57 N. Nishimura, V. Gray, J. R. Allardice, Z. Zhang, A. Pershin, D. Beljonne and A. Rao, *ACS Mater. Lett.*, 2019, **1**, 660–664.
58 A. Wisetsai, R. Lekphrom and F. T. Schevenels, *Nat. Prod. Res.*, 2021, **35**, 1582–1589.
59 I. Fonseca, R. Larissa, S. Foltran, M. Helmer, L. Marcelo, H. Gehlen, R. Lopes, D. Carlos and R. Duarte, *J. Fluoresc.*, 2021, 1417–1424.
60 W. Tomal, M. Pilch, A. Chachaj-Brekiesz, M. Galek, F. Morlet-Savary, B. Graff, C. Dietlin, J. Lalevée and J. Ortyl, *Polym. Chem.*, 2020, **11**, 4604–4621.
61 M. Topa, F. Petko, M. Galek, M. Jankowska, R. Popielarz and J. Ortyl, *Eur. Polym. J.*, 2021, **156**, 110612.
62 C. Hofstetter, S. Orman, S. Baudis and J. Stampfl, *Addit. Manuf.*, 2018, **24**, 166–172.
63 Y. Li, Q. Mao, J. Yin, Y. Wang, J. Fu and Y. Huang, *Addit. Manuf.*, 2021, **37**, 101716.
64 M. Sangermano, N. Razza and J. V. Crivello, *Macromol. Mater. Eng.*, 2014, **299**, 775–793.
65 N. Guy, O. Giani, S. Blanquer, J. Pinaud and J. J. Robin, *Prog. Org. Coat.*, 2021, **153**, 106159.
66 A. A. Pérez-Mondragón, C. E. Cuevas-Suárez, J. A. González-López, N. Trejo-Carbajal and A. M. Herrera-González, *J. Photochem. Photobiol., A*, 2020, **403**, 112844.
67 T. Gencoglu, T. N. Eren, J. Lalevee and D. Avci, *J. Photochem. Photobiol., A*, 2021, **404**, 112959.
68 J. Christmann, X. Allonas, C. Ley and C. Croutxé-Barghorn, *Polym. Chem.*, 2019, **10**, 1099–1109.
69 R. Podsiadły, K. Podemska and A. M. Szymczak, *Dyes Pigm.*, 2011, **91**, 422–426.
70 S. H. Messaddeq, A. S. Bonnet, S. H. Santagnelli, G. Salek, Y. N. Colmenares and Y. Messaddeq, *Mater. Chem. Phys.*, 2019, **236**, 1–9.
71 I. Q. A. Amir, S. S. Hashim and S. H. Guzar, *Mater. Today: Proc.*, 2022, **60**, 1741–1746.
72 Z. Czech, A. Kowalczyk, J. Ortyl and J. Świderska, *Pol. J. Chem. Technol.*, 2013, **15**, 12–14.

